Numerical Investigation of Scale Effect of Various Injection Diameters on Interaction in Cold Kerosene-fueled Supersonic Flow

Lin Zhu[1], Yin-Yin Qi[1], Wei-Lai Liu[2*], Bao-Jian Xu[2], Jia-Ru Ge[1], Xiang-Chun Xuan[3], Tien-Chien Jen[4]

1. Mechanical Engineering Department, Anhui Agricultural University, Hefei, 230036, China

2. Department of Precision Machinery & Precision Instrumentation, University of Science & Technology of China, Hefei, 230027, China

3. Department of Mechanical Engineering, Clemson University, Clemson, SC 29634, USA

4. Mechanical Engineering Department, University of Johannesburg, Johannesburg, 2006, South Africa

Abstract

The incident shock wave generally has a strong effect on the transversal injection field in cold kerosene-fueled supersonic flow, possibly due to its affecting the interaction between incoming flow and fuel through various operation conditions. This study is to address scale effect of various injection diameters on the interaction between incident shock wave and transversal cavity injection in a cold kerosene-fueled scramjet combustor. The injection diameters are separately specified as from 0.5 to 1.5mm in 0.5mm increments when other performance parameters, including the injection angle, velocity and pressure drop are all constant. A combined three dimensional Couple Level Set & Volume of Fluids (CLSVOF) approach with an improved K-H & R-T model is used to characterize penetration height, span expansion area, angle of shock wave and sauter mean diameter (SMD) distribution of the kerosene droplets with/without considering evaporation. Our results show that the injection orifice surely has a great scale effect on the transversal injection field in cold kerosene-fueled supersonic flows. Our findings show that the penetration depth, span angle and span expansion area of the transverse cavity jet are increased with the injection diameter, and that the kerosene droplets are more prone to breakup and atomization at the outlet of the combustor for the orifice diameter of 1.5mm. The calculation predictions are compared against the reported experimental measurements and literatures with good qualitative agreement. The simulation results obtained in this study can provide the evidences for better understanding the underlying mechanism of kerosene atomization in cold supersonic flow and scramjet design improvement.

Key words: Scale effect, Transversal cavity injection, Cold supersonic flow, Couple Level Set & Volume of Fluids (CLSVOF), K-H & R-T model

1. Introduction

Development of an optimum supersonic combustion ramjet (scramjet) engines are pivotal for the realization of hypersonic vehicles [1]. Understanding the effect of the injection system design on the interaction characteristics between incoming flow and fuel in cold supersonic flow is a key issue for development of scramjets. However, design of the optimum injection system with great performance capabilities is really a challenge [2]. This is predominantly due to the fact that the hypersonic vehicles are generally operated at high Mach number, e.g. 8, which indicates that the residence time of the supersonic free-stream within the combustion chamber of the scramjet is extremely short, typically on the order of milliseconds [1]. Too short residence time of the fuel incurs incomplete mixing and, hence, strongly affects the combustion efficiencies [2].

Currently, studies have already addressed the design of injector systems for improving the fuel-air mixing

characteristics. For example, transversal fuel injection through a wall orifice is considered to be one of the simplest and most conventional approaches for the scramjet engine, possibly due to its good fuel penetration, interaction, and mixing [3-6]. Abdelhafz et al. [7] numerically investigated oblique and transverse configurations when gaseous fuel was injected into a low-aspect-ratio supersonic combustor. They claimed that injecting fuel obliquely can result in higher mixing efficiencies. Huang et al [8] addressed the effect of injection angle of helium, under various pressure conditions, on the interaction between fuel and incoming air in the transversal injection flow field. They concluded that RNG $k-\varepsilon$ turbulence model is better in predicting the wall pressures under low jet-to-crossflow pressure ratios, whilst SST $k-\varepsilon$ is more appropriate for high jet-to-crossflow pressure ratios. Since a counter-rotating vortex pair appears behind a jet, fuel–air mixing is induced by jet penetration into supersonic crossflow. S.H. Lee et al. [9-12] proposed multiple injections to enhance the fuel-air mixing characteristics. A. Zang et al. [13] found out that a cavity model can also improve the characteristics of air mixing, and it has been investigated as a flame holding mechanism for the scramjet engine [14-15]. However, to the best of our knowledge, there are few studies in literature for the fuel-air mixing characteristics in a cold kerosene-fueled supersonic flow. A careful study of fuel-air interaction is essential to better understand the underlying mechanism of kerosene atomization in cold supersonic flow as well as the scramjet design improvement.

Hence, in this study we are concerned to numerically investigate the scale effect of varying injection diameters, in a cold kerosene-fueled scramjet combustor, on the interaction between incident shock wave and transversal cavity injection using a combined three dimensional Couple Level Set & Volume of Fluids (CLSVOF) approach with an improved K-H & R-T model.

2. CFD Model and Simulation Approach

2.1. Model geometry

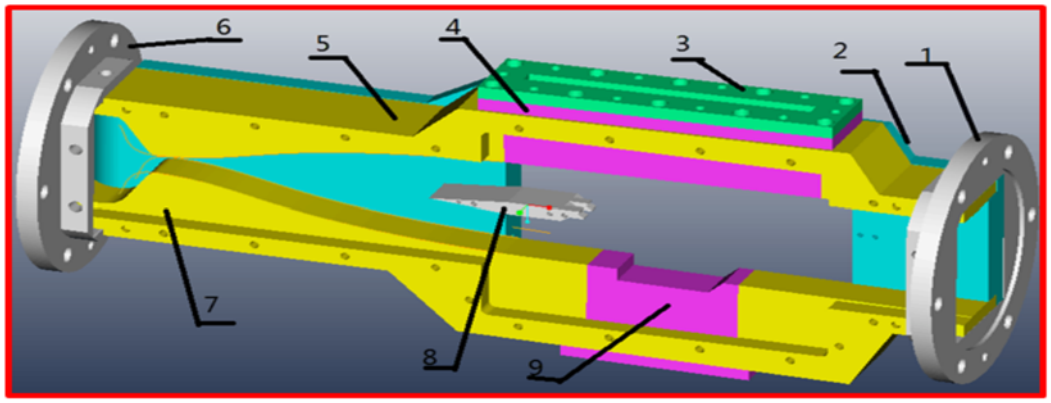

Fig. 1. Schematic of a scramjet combustor: 1. flange, 2. rear cover, 3. pressure pad of upper glass window, 4. upper glass window, 5. upper cover, 6. flange, 7. lower cover, 8. Strut, 9.cavity

Figure 1 schematically illustrates the real prototype of scramjet combustor presented by Liu [16]. In the original design, for the purpose of experimental measurements, the scramjet combustor contains flange 1 and 6, pressure pad of upper glass window 3 and upper glass window 4. To simply the CFD model, however, the foregoing components are ignored because they do not affect the interaction between kerosene and supersonic flow. Though the strut 8 affects the flow patterns of the mixture in the combustor, it is not consider either due to the fact that there is not the component in the present experimental setup of Liu's. As a result, the scramjet combustor in this study consists of rear cover 2, upper cover 5, lower cover 7 and cavity 9. Figure 2 shows the simplified geometry of the three-dimensional scramjet combustor by using a combined feature-based modeling approach and Virtual Assembly Technique (VAT) [17]. The primary specifications used for the calculation are listed in Table.1. Note that the incident

shock wave, generated by kerosene, is injected from the orifice at the center of the cavity (see Fig. 2 (b)).

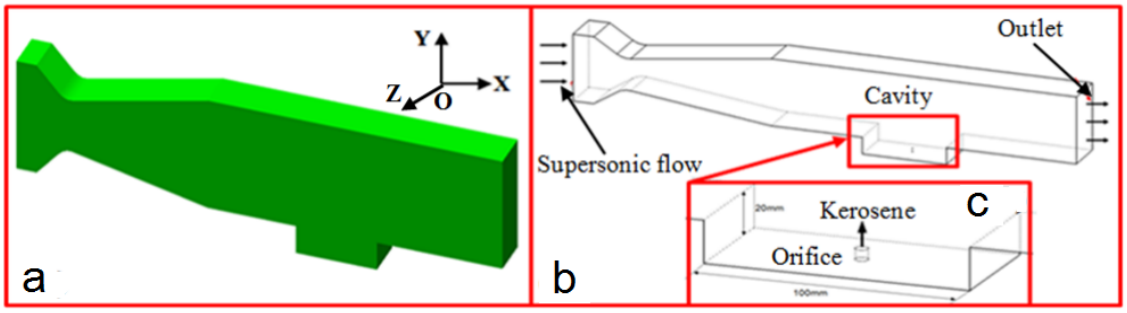

Fig.2. (a) A three-dimensional model of the scramjet combustor, (b) Computational domain of (a) and (c) the cavity configuration

Table 1

Specifications of the scramjet combustor

Item	Dimension
Scramjet combustor	$0.6\times0.05\times\times0.08m^3$ (length×width×height)
Cavity	$0.1\times0.05\times0.02$ m^3(length×width×height)
Orifice	(0.5, 1 and 1.5×10^{-3}m) ϕ, 0.02m long
Inlet & outlet	$0.05\times0.08m^2$(width×height)

2.2. CFD modeling

Figure 3 shows the meshed CFD model of the scramjet combustor. There are totally 330,000 hexahedron cells used for the combustor, in which the mesh cells are concentrated around the walls and the region near the cavity due to the strong interaction between incident shock wave and transversal cavity injection.

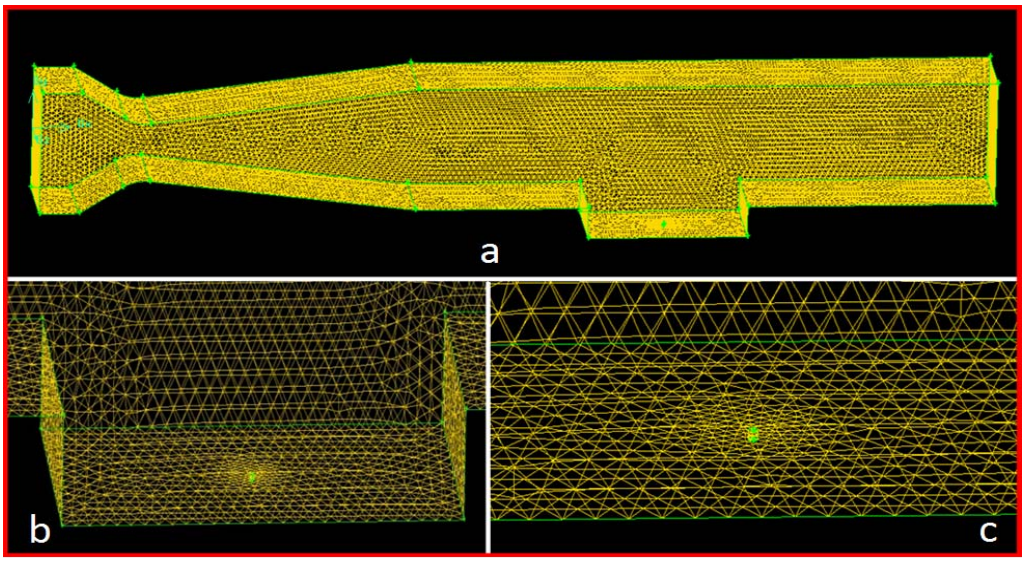

Fig.3. Details of numerical grid of the scramjet combustor

The interaction between incoming flow and kerosene was simulated by commercial CFD software ANSYS Fluent 14.0 to understand the interface breakup and coalesce with another interface. As for this, Volume of Fluids (VOF) model is generally used for the underlying physical mechanisms [18]. However, additional re-meshing is

necessitated when VOF is applied for a large deformation of the gas-liquid interface [18]. The mixing process of incident shock wave and transversal cavity injection in supersonic flows generally results in more complex turbulent structures [19]. Hence, in this study three dimensional Couple Level Set & Volume of Fluids (CLSVOF) model was proposed to predict the scale effect of various injection diameters on the breakup behaviors of kerosene droplets in the cold kerosene-fueled scramjet combustor. This may be explained as due to CLSVOF coupling the LS (Level Set) and VOF. In detail, CLSVOF model contains the advantage of VOF: automatically deal with topological changes with a higher-order of accuracy, and also overcomes the disadvantage of VOF: unable to accurately compute such important properties as the curvature and the normal to the interface [20]. Consequently, CLSVOF is more accurate than both the standalone LS and VOF models [20]. Note that the LS and VOF methods belong to one fluid method. A single set of the conservation equation is therefore used for the whole domain, and there are no separate gas-liquid velocities. In this case the Navier-Stokes has the following form [20]:

$$\int_v \frac{\partial(\rho u)}{\partial t} + \int_v \nabla \bullet (\rho u \otimes u) = -\int_v \nabla p + \int_v \nabla \bullet (2\mu D) + \int_v F_{st} + \int_v \rho g \tag{1}$$

and the continuity equation is

$$\int_v \frac{\partial \rho}{\partial t} + \int_v \nabla \bullet (\rho \vec{V}) = 0 \tag{2}$$

where $\vec{V}$ is the velocity vector, ρ is the fluid density defined by Eq. (3), t is the time, μ is the fluid viscosity defined by Eq. (4), D is the viscous deformation tensor defined by Eq. (5), g is the gravity vector and the body force due to the surface tension, F_{st}, is defined using the immersed boundary method to represent the presence of the solid surface in the fluid. We refer the readers to the work of Yu (2007) [21] and T. Mènard (2007) [22] for details of the equations (3) ~ (5) and the implementation of the immersed boundary method.

$$\rho(\Phi) = \rho_1 - (\rho_1 - \rho_g) H(\Phi) \tag{3}$$

$$\mu(\Phi) = \mu_1 - (\mu_1 - \mu_g) H(\Phi) \tag{4}$$

$$D = 1/2(\nabla V + \nabla V^T) \tag{5}$$

In addition, both energy equation and the state equation of the gaseous mixture were also taken into account in this study. The detailed formulas are presented as follows:

The energy equation for a droplet is [23]:

$$\mathrm{m}\frac{de}{dt} = q + Q_s \tag{6}$$

where $e = c_{vs}T_s + h_f^0$, $Q_s = \frac{dm}{dt}h_L$ —the energy of phase transitions, c_{vs} —specific heat capacity, h_L —the latent heat of evaporation, q —heat flux to a single droplet from the surrounding gas flow. It is determined by the following forms[24]:

$$q = \begin{cases} \pi d \lambda g Nu g (T - T_s) & R_e < 1000 \\ \pi d^2 \rho \left| \vec{v} - \vec{u} \right| g St g (H_r - H_w) & R_e \geq 1000 \end{cases} \tag{7}$$

where $Nu = 2 + 0.16\mathrm{gRe}^{2/3}\mathrm{gPr}^{1/3}$, $S_t = \frac{C_d}{2}\mathrm{Pr}^{-2/3}$, $\vec{u} = \frac{d\vec{r}}{dt}$ —fluid velocity vector, $\vec{r}$ —droplet coordinate, $\vec{v}$ —droplet velocity, T—gas temperature, T_s—droplet temperature.

The state equations for gaseous mixture has the following form [25]

$$p = R_g \rho T \sum_k Y_k / W_k$$

$$E = \sum_k Y_k (c_{vk} T + h_{ok}) + \vec{u}^2/2 + k \tag{8}$$

where E is the gas energy, k—the turbulent kinetic energy, W_k—the molar mass of the kth gas component, h_{ok}—the specific chemical energy, c_{vk}—the specific heat capacity, Y_k—the mass concentration of the kth gas component, T—the gas temperature, R_g—the universal gas constant.

For all simulations reported in this paper, the pressure-based (coupled) double precision solver was used to solve the governing equations, i.e. Reynolds averaged Navier-Stokes (RANS) equations. The boundary conditions for the CFD modeling were defined to mostly match the experimental scenarios reported by Liu so that the simulation results can be compared with those from the coming tests. Since the model ignored the flange, uniformly distributed speed, pressure and temperature were assumed on the air inlet. The strut was not considered in this study due to no related component available in the present experimental setup. Thus, the airflow model around the strut was not considered in the current predictions.

In the present study, the turbulence was modeled using Menter's two-equation shear stress transport (SST) k-ω model [26]. This is because the SST model combines the advantages of the k-ω model near solid surfaces with the k-ε model. Consequently, this model is less sensitive to the specification of free stream turbulence level compared with the k-ω model and performs comparatively well in adverse pressure gradients and separated flows. Moreover, the SST model has been used successfully for transverse injection flow in previous studies [27]. Following the foregoing turbulence model, the turbulence characteristic values used here were: turbulence intensity—8%, hydraulic diameter—0.5, 1.0, 1.5mm. In addition, the courant-Friedrichs-Levy (CFL) number remained at 0.5 with suitable under-relaxation factors to ensure stability.

For the coming air, it was assumed to be a thermally and calorically perfect gas, and the mass-weighted-mixing law of viscosity was utilized; the key operation properties were separately set to be a Mach number of 2.2 and a stagnation pressure P_0 of 7.85 MPa. For kerosene jet flow, the performance parameters were specified as an injection velocity of 70ms^{-1}, injection angle of 90°, and injection pressure drop of 2MPa, respectively. At the inlet and outlet of the scramjet combustor, a fixed pressure of 1.013×10^5 Pa was specified. At the wall no-slip boundary conditions were used for the channel wall, in which the standard wall functions defined in FLUENT were applied to model the near-wall region flow. The stagnation temperature T_0 was designated as 300K. The other parameters of kerosene, e.g. density ρ=0.78 g/cm^3, viscosity u=2$mPa \bullet s$, and surface tension σ=$23.6*10^{-3}$ N/m were also included.

3. Results and Discussion

In this section, the 3D scramjet combustor, previously depicted from Liu's experiment, is tested numerically to characterize the mixing between incident shock wave and transversal cavity injection, i.e. the kerosene atomization, in a cold supersonic cross airflow. The mixing characteristics under the different kerosene-injecting diameters are carefully investigated through the following four key behaviors of droplets, e.g. penetration depth, span expansion area, angle of shock wave and sauter mean diameter (SMD) distribution.

3.1. Numerical accuracy

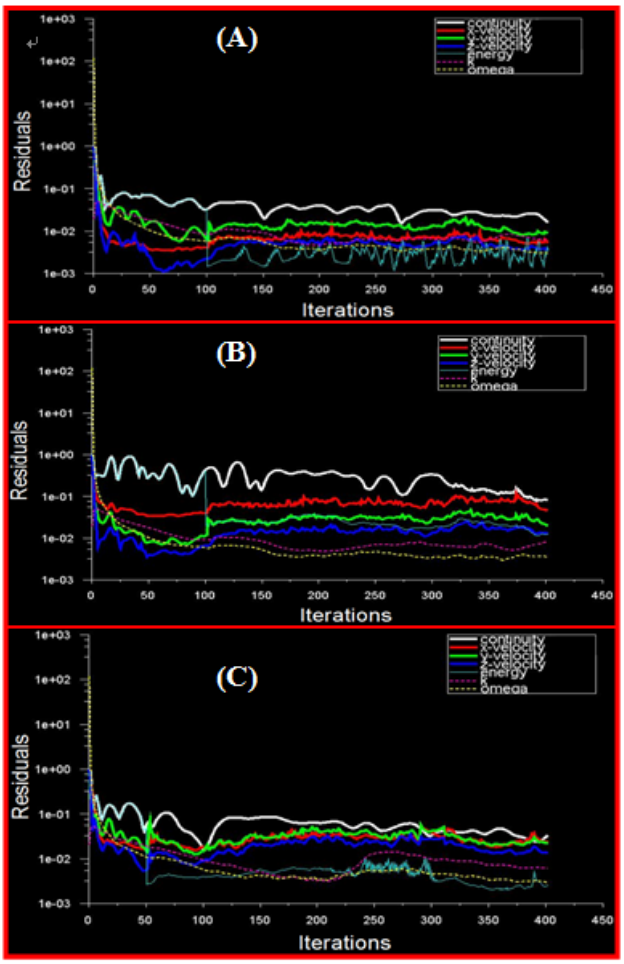

Fig.4. Residual variation with iteration number under various injection diameters (A) 0.5mm, (B)1.0mm and (C) 1.5mm

The grid-dependency study demonstrated that the grid scale has a slight effect on the transverse injection flow field in supersonic flows [28]. As such, as depicted in section 2.2, the medium sized domain (330,000 hexahedron cells) was considered to be sufficient to produce analogous results for the current numerical predictions [28].

The method of convergence and discretization error analysis used in this study is based on previous numerical investigations [29]. In detail, the computational model is believed to reach a state of convergence once the residuals for the flow field parameters (such as continuity, momentum, etc.) fall below a certain order of magnitude.

For all simulations in this study, the solution convergence is judged according to the residuals of the governing equations. The numerical results reported were based on the criteria that when the residual of each equation is smaller than 1.0×10^{-3}, the computations are stopped and remain stable. The average time step was around 10 μs, and a typical run actually took 2107 time steps to simulate a real time of about 21 ms. Figure 4 shows the residual variations of different flow field parameters with the iteration number, in which the primary operation parameters include

continuity, velocity, energy, k and omega for the computational domain. The k and Omega are both the flow parameters related with the used viscous model, i.e. SST $k-\varepsilon$. As observed, the literation number for the injection diameters of 0.5mm, 1.0mm and 1.5mm are approximately 450, when the computational model of the scramjet is in convergence. Note that the situation that all but energy is less than a certain value, e.g. 10^{-3} is also considered to be converged [28].

3.2. Penetration height

Figure 5 shows the penetration heights of the kerosene jet, in the scramjet combustor (Fig. 2), under the different injection diameters. For different injection diameters, the main flow structures obtained herein are identified, which includes primary compression shock, compression shock normal to the wall and curved central compression shock. These are in qualitative agreement with [30]. Furthermore, as observed along the Y direction, for orifice diameter of 0.5mm, most of the kerosene droplets are located in the range of -40 to 10 mm, far away from the outlet of the combustor (Fig. 5 (a)); for 1.0mm orifice diameter, some of the droplets lie at the outlet between 10 mm and 25mm (Fig. 5 (b)); when the injection diameter is increased to 1.5mm, the majority of the droplets appear at the outlet , i.e. ranging from 0 to 35mm (Fig. 5 (c)). It is therefore inferred that at the identified injection velocity, angle and pressure drop the penetration height of the kerosene droplets increases when the injection diameter is increased. This can be explained as follows: an increase in injection diameter results in an increase in total momentum of liquid jet from the orifice and, hence, in inertia force of liquid jet. The increased inertia force causes the liquid jet to deflect difficultly, thereby enlarging its penetration height.

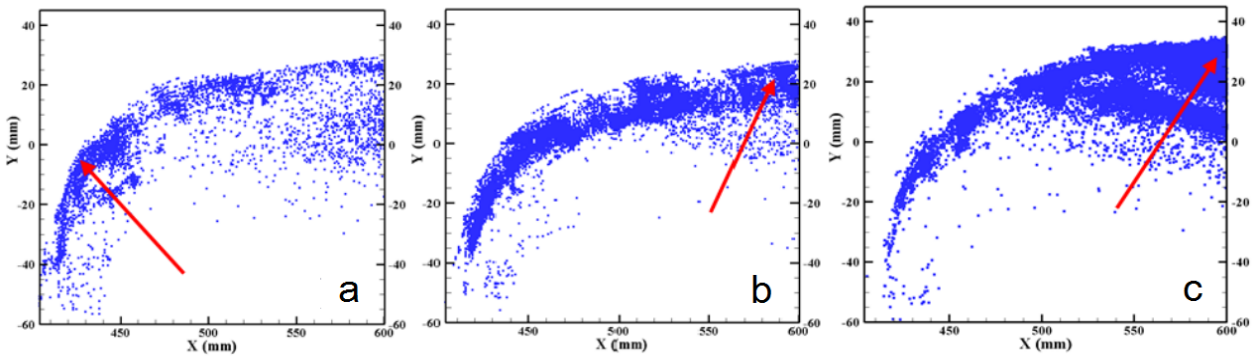

Fig.5. Penetration heights of the kerosene jet under the different injection diameters (a) 0.5mm, (b) 1.0mm and (c) 1.5mm

3.3. Span expansion area

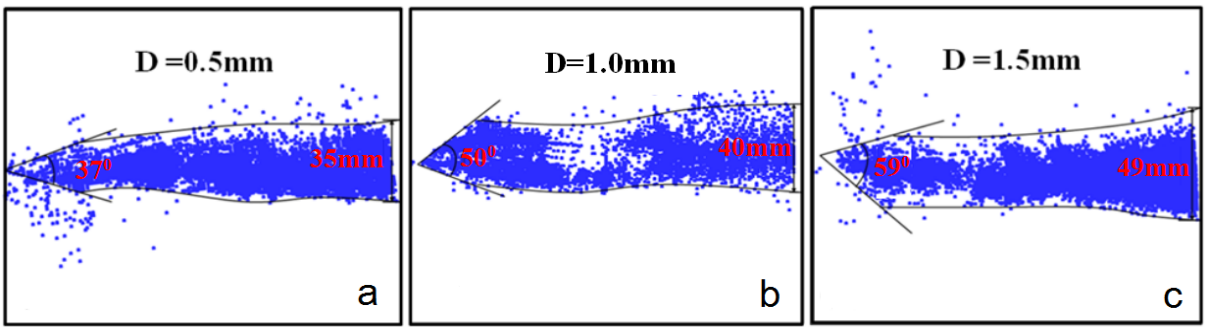

Fig.6. Span-wise expansion area of the kerosene jet under the different injection diameters

Figure 6 shows the span expansion variation of the kerosene jet, within the plane XOZ in the scramjet combustor, with the injection diameter ranging from 0.5mm up to 1.5mm. The span expansion area is 60 mm vertically away

from the orifice in the cavity shown in Fig. 2. As observed, when the injection diameters are separately 0.5, 1.0 and 1.5mm the span area of the kerosene jet is increased. The expansion breadths and angles of the kerosene jet in the plane XOZ approximately increase from 35 mm, 37° to 40 mm, 50° and 49 mm, 59°, respectively. This may possibly be attributed to the fact that an increase in injection diameter is accompanied with an increase in flow rate of the kerosene jet. The more flow rate in turn results in the greater expansion breadth and angle of the span area.

3.4. Angle of shock wave

Figure 7 shows the angle of shock wave of the kerosene jet from the orifice in the cavity when the injection diameter varies. When the orifice diameter is increased from 0.5 to 1.5mm, as shown in Fig. 7, the shock wave angle is increased from 57° to 65° and 69°, respectively. Furthermore, the injection distance of the kerosene droplets, at the outlet of the combustor shown in Fig. 2, is also separately increased from 26 to 29 and 38 mm. The foregoing results are in good agreement with those in Fig. 5. It is therefore concluded that kerosene droplets are prone to mixing with incoming flow and atomization with an increase in shock wave angle. This phenomenon can be explained by the increase in total momentum of liquid jet from the orifice and, hence, in inertia force of liquid jet. Generally, the increased inertia force causes the liquid jet to deflect difficultly, thus enlarging the shock wave angle of kerosene jet.

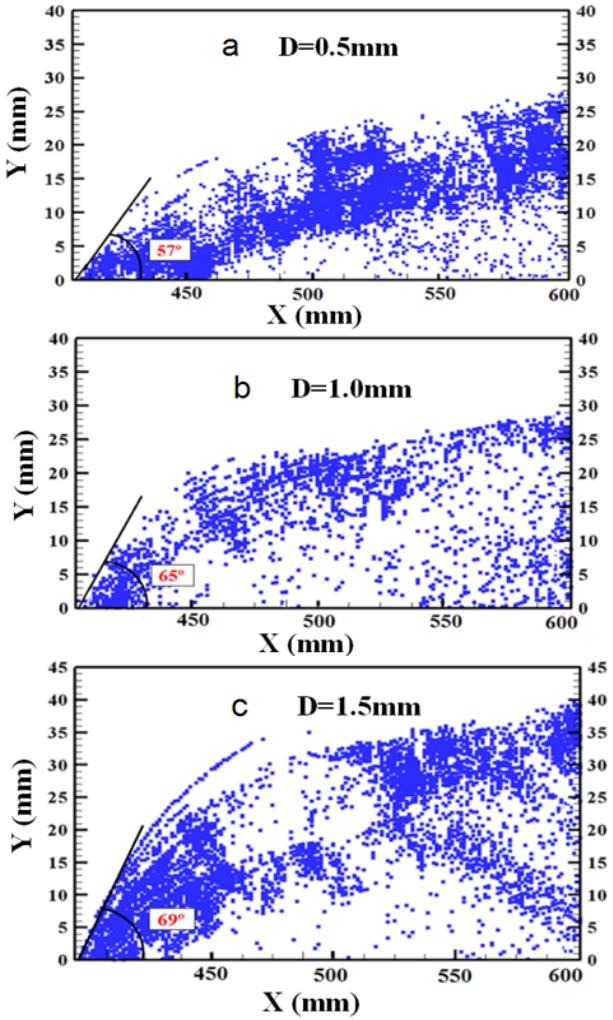

Fig.7. Angle of the shock wave of the kerosene jet under the different injection diameters

3.5. Sauter mean diameter (SMD) distribution

As for the droplet atomization supplied by SMD distributions, for simplicity Blob model was utilized for the primary atomization, in which the droplet size was designated as the injection diameter, i.e. 0.5, 1.0 and 1.5mm, respectively [31]; an improved K-H & R-T model, i.e. K-H & R-T model II was used for the description the droplets' breakup due to the fact that the numerical results using the foregoing model are in good agreement with the experimental evidences at the same settings in supersonic crossflow [31~32].The detailed description on K-H & R-T model II is presented as follows: according to [31], firstly, the shear interaction occurs between liquid jet and supersonic flow as the liquid jet injects from the orifice, when K-H wave appears on the liquid jet and so many droplets peel off from the liquid jet. Thus, K-H model is appropriate to calculate the process. Then, as the liquid jet enters into the combustion chamber, droplets continuously peel off the liquid jet and most importantly, the peeled droplets break up. It is true to consider the foregoing phenomenon affected by both K-H wave and R-T wave. For this reason, a combined K-H and R-T model, i.e. K-H & R-T model II is better to characterize the process. However, there is another important issue to determine, or the time when the R-T model is incorporated into K-H model for calculating the atomization process of the droplets. The related formulas for the above description are [32]:

1) K-H model

$$\frac{\Lambda}{r}=9.02\frac{(1+0.45Oh^{0.5})(1+0.4T^{0.7})}{(1+0.87We_g^{1.67})^{0.6}} \tag{9}$$

$$\left[\frac{\Omega\rho_d r^3}{\sigma}\right]^{0.5}=\frac{0.34+0.38We_g^{1.5}}{(1+Oh)(1+1.4T^{0.6})} \tag{10}$$

wher Λ is the surface wave length of liquid jet at the maximum growth rate Ω, $Oh=\sqrt{We_d}/\mathrm{Re}_d$ —Ohnesorge number of droplet, $We_d=\rho_d r v^2/\sigma$ —Weber number of droplet, $Re_d=rv/v_d$ —Reynolds number of droplet, ρ_d —the density of liquid jet, $v=|\mu_d-\mu_g|$ —the relative velocity between droplet and gas, r—the radius of droplet, ρ_g —the density of gas, σ is the surface tension at the interface , We_g —Weber number of gas, $T=\sqrt{We_d}Oh$.

The mean radius of droplets r* after breakup can be determined by

$$\mathrm{r}^*=\begin{cases} B_0\Lambda & B_0\Lambda\le r \\ \min\begin{cases}(3\pi r^2 v/2\Omega)^{0.33}\\ (3r^2\Lambda/4)^{0.33}\end{cases} & B_0\Lambda>r\end{cases} \tag{11}$$

The breakup velocity of droplets is

$$\frac{dr}{dt}=-\frac{(r-r^*)}{\tau_b} \tag{12}$$

where $\tau_b=3.726B_1 r/\Lambda\Omega$; B_0 , B_1 are constant, $B_0=1.22$, $B_1=30$.

2) R-T model

$$\Omega_{RT}=\sqrt{\frac{2}{3\sqrt{3\sigma}}\frac{[-g_d(\rho_d-\rho_g)^{3/2}}{\rho_d+\rho_g}} \tag{13}$$

where Ω_{RT} is a frequency of an unsteady wave at the maximum growth rate, g_d — an acceleration of droplets

The wave number K_{RT} is

$$K_{RT} = \sqrt{\frac{-g_d(\rho_d - \rho_g)}{3\sigma}} \tag{14}$$

The breakup time for droplets τ_{RT} is

$$\tau_{RT} = \frac{C_\tau}{\Omega_{RT}} \tag{15}$$

The mean radius of droplets r* after breakup is

$$r^* = \frac{\pi C_{RT}}{K_{RT}} \tag{16}$$

where C_τ, C_{RT} are constant; $C_\tau = 1, C_{RT} = 0.35$ in this study.

3) Time criterion on incorporating R-T model into K-H model

As discussed previously, as the liquid jet enters into the combustion chamber, droplets continuously peel off from the liquid jet and the peeled droplets break up. This is caused by a combined effect of both K-H wave and R-T wave. Due to the fact that either the breakup of droplets or the split of liquid jet is caused by the drag forces of gas, the criterion ,i.e. time scale herein can be determined based on [32]

$$\left.\begin{aligned} t_b / t^* &= 5.0 \\ t^* &= d_d \sqrt{(\rho_d / \rho_g)} / v \end{aligned}\right\} \tag{17}$$

where t_b is the breakup time of droplets, t^* —the characteristic time, d_d —the diameter of droplet.

According to formula (17), if $t < t_b$, the breakup of droplets is calculated using K-H model, whilst if $t \geq t_b$, it is simulated by a competing effect of K-H and R-T models. The advantages of the criterion are that 1) it can be used at various gas velocities and in the wide range of Weber number, e.g. 10^2~10^6 and 2) it has most simple form and even do not need any experimental values for numerical prediction [32].

In addition, in order to provide the true data for evaluating mixture quality, the evaporation of kerosene droplets was also taken into account in all simulations. Due to the non-uniformity interaction between fuel and air in supersonic cross flow, the non-equilibrium evaporation model was utilized to determine the evaporation rate [32, 33]

$$\dot{m} = \pi d g \rho_g D g N \mu g \log(1 - Y_e / 1 - Y_w) \tag{18}$$

where d is the diameter of droplet, ρ_g —the density of gas, D—mass diffusion coefficient, $N\mu$ —Nusselt number of mass transfer, $Y_w = \frac{W_N P_0}{W_p} \exp[\frac{H_b}{R}(\frac{1}{T_b(P_0)} - \frac{1}{T_s})] - \dot{m}\frac{\sqrt{2\pi RT_s}}{\pi \delta_e p d^2}$. We refer the readers to the work of Nickolay N.Smirnov [33] for details of the above expression. For the foregoing evaporation model, the related thermal characteristics for gas and droplets are: ambient pressure p=1.013×10^5 Pa, Initial droplet temperature — T=300K, static temperature of gas (considering evaporation) — T=536K, gaseous phase—air, liquid—kerosene, mass diffusivity (m^2/s) —2.88×10^{-5}, thermal conductivity (W/m·k) —0.0454, the latent heat of evaporation h_L —226kj/kg.

Figures 8 and 9 separately show the sauter mean diameter (SMD) distributions of the kerosene droplets without/with the evaporation of kerosene along the x direction, as shown in Fig.2. These were based on the different injection diameters, i.e. 0.5, 1.0 and 1.5mm. Note that the SMD distribution herein indicates the kerosene droplet

distribution at the cross-section vertical to the supersonic flow direction (Fig.11). The distance in Figs. 8~10, i.e. 50, 100, 150 and 200mm is the length between cross-section and orifice in the cavity.

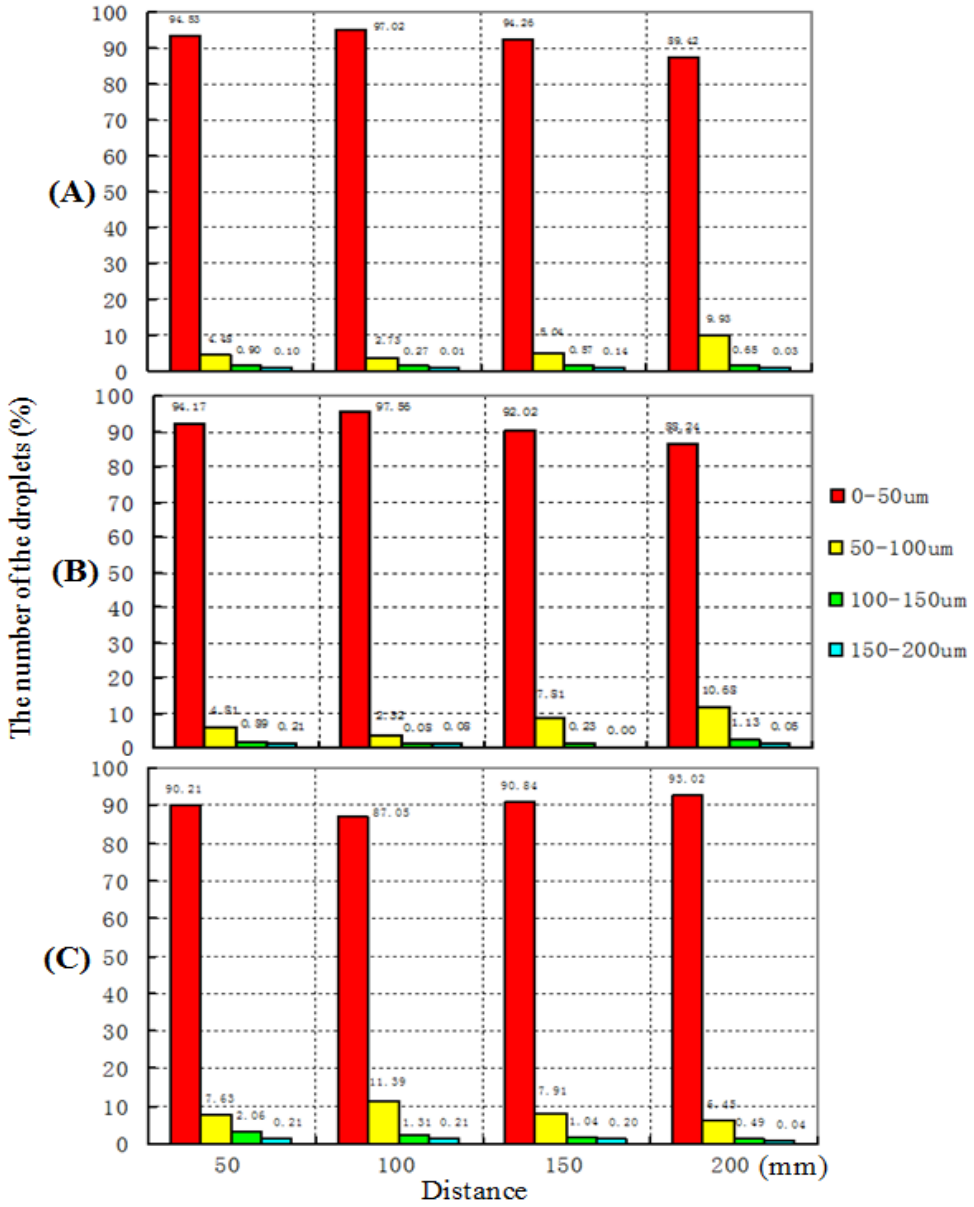

Fig.8. SMD distribution of the kerosene droplets under the different injection diameters (A) 0.5mm, (B) 1.0 mm and (C) 1.5mm without considering evaporation

Figure 8 shows the SMD distribution of the kerosene droplets, along the x direction, under the different injection diameters without considering evaporation. As observed, when the injection diameter is increased from 0.5 to 1.5mm the concentration of the kerosene droplets gradually varies along the x direction. One interesting finding is that without the evaporation 94.53% of the smallest droplets (0~50 um) appears at the location, about 50mm away from the orifice, when the injection diameter is 0.5 mm, and that when the injection diameter is increased to 1.5mm about 93.02% of the 50 um droplets are located at the region, 200mm far from the orifice, right at the outlet of the combustor. Note that 94.53%, 93.02% are separately accounted for the smallest droplets of all kerosene jets in this study. As such, it is inferred that the injection diameter in the combustor is strongly accompanied with the number of the smallest kerosene droplet. This can basically be explained as due to the fact that an increase in injection diameter results in an increase in total momentum of liquid jet from the orifice. The greater momentum generally causes the greater concentration of the smallest kerosene droplet. This can also schematically be demonstrated by Fig.11, which presents

the velocity distributions of the kerosene droplets, along the cross-section vertical to the air-stream direction, under the different injection diameters, i.e. 0.5mm, 1.0mm and 1.5mm. At the outlet of the combustor, as observed, the expansion area of the kerosene droplets with high speed in Fig. 11 (c) is really greater than those in Figs. 11 (a) and (b).

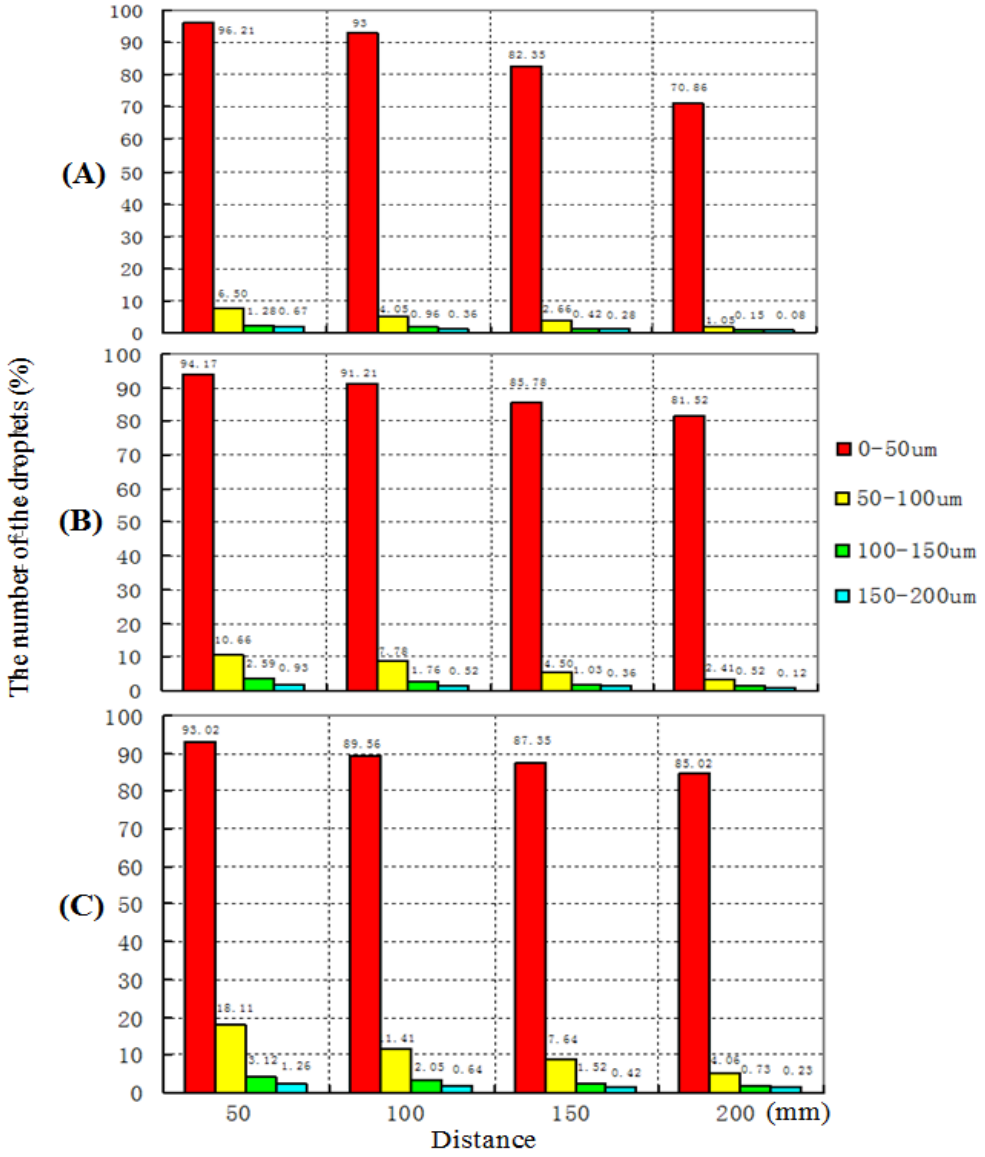

Fig.9. SMD distribution of the kerosene droplets under the different injection diameters (A) 0.5mm, (B) 1.0 mm and (C) 1.5mm with considering evaporation

Figure 9 shows the SMD distribution of the kerosene droplets, along the x direction, under the different injection diameters with evaporation. As observed, for the injection diameters of 0.5 and 1.5mm, about 96.21% and 85.02% of the smallest droplets appear at the identified positions with those in Fig.8. Compared the number of the kerosene droplets (0~50um) without evaporation and that with evaporation, it is further seen that for the injection diameter of 0.5mm, the number of the smallest droplets reduces from 89% without evaporation to 71% with evaporation at the outlet of the combustor, whilst for the injection diameter of 1.5mm, at the outlet the number reduces from 93% to 85% (Fig.10). Consequently, it is concluded that evaporation also strongly affects the droplet breakup. This may be explained as due to the fact that evaporation causes the broken-up droplets to gradually disappear during the interaction of fuel and air. From the foregoing analysis, it is therefore concluded that the injection diameter in the combustor is strongly accompanied with the number of the smallest kerosene droplet. The injection diameter therefore

has a great scale effect on the injection breakup and, hence, on the droplet atomization in cold supersonic flow. The breakup condition of the kerosene droplet is based on the fact that the lower concentration of kerosene indicates the smaller diameter of the droplet [34]. This can basically be attributed to the fact that an increase in injection diameter results in an increase in total momentum of liquid jet from the orifice. The greater momentum generally causes the greater concentration of the smallest kerosene droplet. Under the effect of evaporation, a wider expansion area appears along the x direction, which is good to improve the mixture quality.

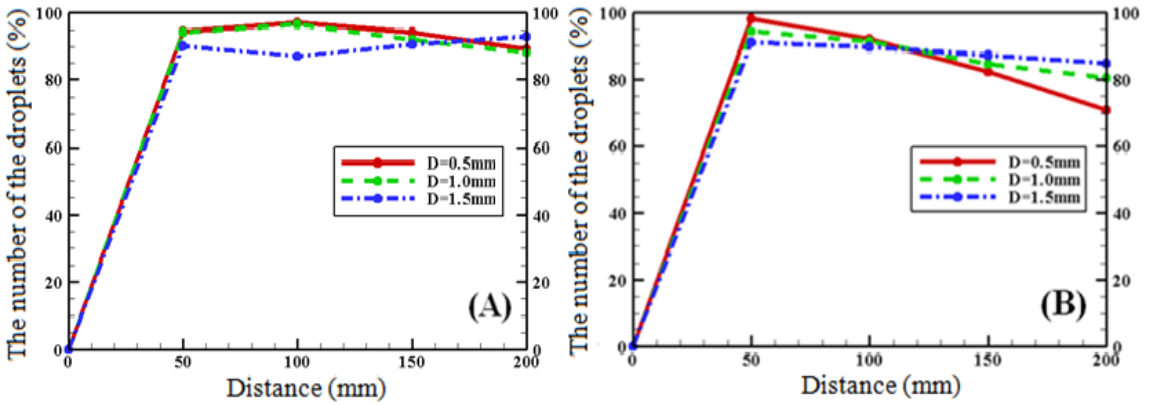

Fig.10. Comparison of the number of the kerosene droplets (0~50um) (A) without and (B) with evaporation

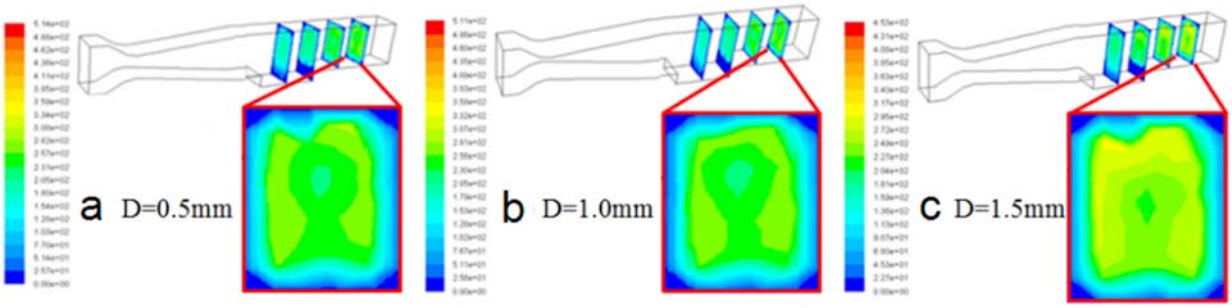

Fig.11. Velocity distribution of the kerosene droplets along the cross-section vertical to the air-stream direction in the combustor (a) 0.5mm, (b) 1.0mm and (c) 1.5mm

4. Comparison of Results with Published Data

Though the numerical predictions in this study are based on the prototype of the 3D scramjet combustor used in Liu's experiment, there are no experimental data available in literature. Hence, in order to verify the CLSVOF-based predictions obtained in this study the mixing characteristics, between incident shock wave and transversal cavity injection, i.e. the kerosene injection in a cold supersonic cross airflow, are compared against the published results. These results were achieved by the following experimental approaches: high speed photography, high speed shadowgraph and particle image velocity (PIV) [35]. The comparisons, including penetration depth, span expansion area and angle of shock wave, are implemented for identified injection angle, i.e. 90^{o} and pressure drop, i.e. 2MPa. The discrepancies between the experimental measurements and this study are 1) 3D model of the scramjet combustor (see Figs. 2 and 12), and 2) injection velocity of the supersonic air-stream. The injection speeds in this study and the measurements are separately 70 ms^{-1} and 63.2 ms^{-1}.

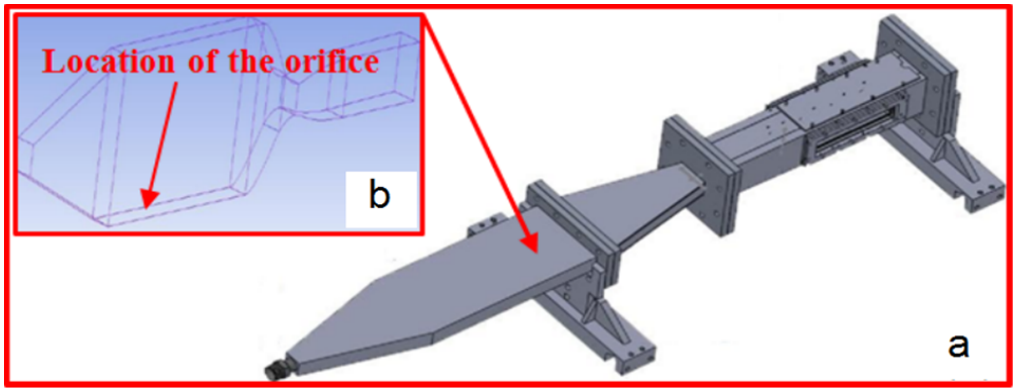

Fig.12. (a) experimental setup of the scramjet combustor; (b) 3D model of the combustor [35]

4.1. Penetration height

Figure 13 shows the boundary curve variations of kerosene jet under different injection diameters (0.4 and 1.0 mm) and pressure drops (0.5, 1, 2, 3, 4 MPa).These experimental evidences came from the original image photos previously obtained by using high speed photography, high speed shadowgraph and particle image velocity (PIV) [35].Compared with the similar scenario in Fig. 5, as observed, there is a qualitative agreement between the numerical predictions in this study and the experimental results in [35]. That is, the penetration height of the kerosene jet trends to increase when the injection diameter is increased. For example, for the pressure drop of 2MPa, as shown in Fig. 13, when the injection diameter D is 0.4 mm, the penetration height of the kerosene jet is measured as 5mm, whilst when D is 1.0 mm the penetration height is approximately increased to 12.5mm. The discrepancy in magnitude between CFD predictions and practical observations can be predominantly due to the different geometric structure of the scramjet combustor. And also it can be attributed to the different operation parameters, e.g. injection speed and diameter. Besides, another comparison is also implemented between Fig.5 and [36]. The qualitative agreement is also found: literature [37] shows that the penetration height is increased with the pressure, and the pressure is considered to be equal to jet velocity. The jet velocity increase indicates the total momentum increase of the liquid jet, which agrees well with section 3.2.

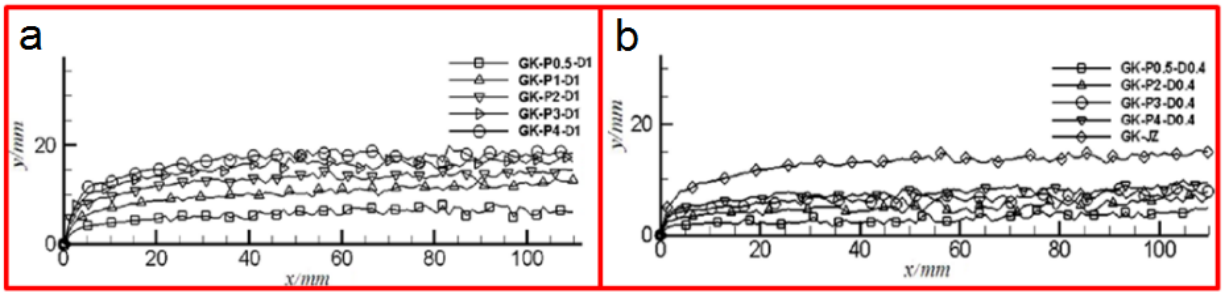

Fig.13. Measured penetration height of liquid jet under different injection diameter (a) 1.0mm and (b) 0.4mm [35]

4.2. Span expansion area

Figure 14 shows the span expansion areas under different injection diameters, i.e.0.4 and 1.0 mm, and identified pressure drop, i.e. 2 MPa. These measurements were achieved at the position of 15mm vertically away from the orifice of the combustor by using a combined high speed photography, high speed shadowgraph and particle image velocity (PIV) with image processing technique[36]. From Figure 14, it can be seen that an increase in span expansion area is accompanied with an increase in injection diameter. For the orifice diameters of 0.4 and 1.0mm, their

expansion width and angle are approximately 20 and 32mm, 16° and 31° , which are in qualitative agreement between the numerical results (Fig. 6).The discrepancy in magnitude between CFD predictions and experimentally measurements is also attributed to the different geometric structure of the combustor and attributed to the different operation parameters.

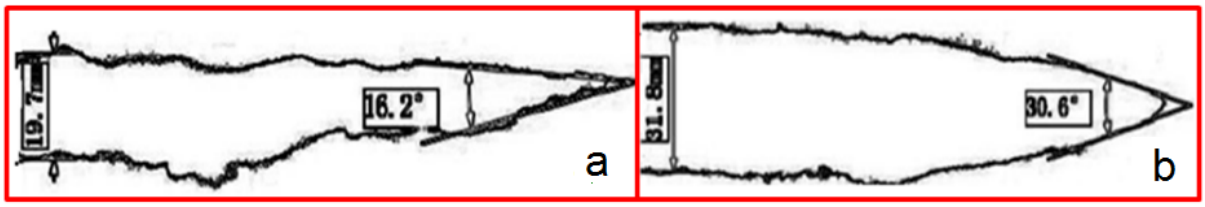

Fig.14. Measured span-wise expansion area under different injection diameter (a) 0.4mm and (b) 1.0 mm [35]

4.3. Angle of shock wave

Figure 15 presents the measured shock wave angle of the kerosene jet when the pressure drop is 2MPa and the injection diameter varies from 0.4 to 1.0mm. The used measurement methods herein are the same as those in Figs.13-14. As observed, the shock wave angle values obtained from the experimental tests are in good qualitative agreement with those predicted by CFD simulations. The angle of shock wave is increased from 35.3° to 39.9° corresponding to the injection diameter of 0.4 and 1.0 mm, respectively. However, another important issue is noted in designing the scramjet combustor that the CLSVOF-based predictions showed that the stronger shock wave incurs the greater total pressure loss (table 2), which was also demonstrated by the experimental evidences in [35].

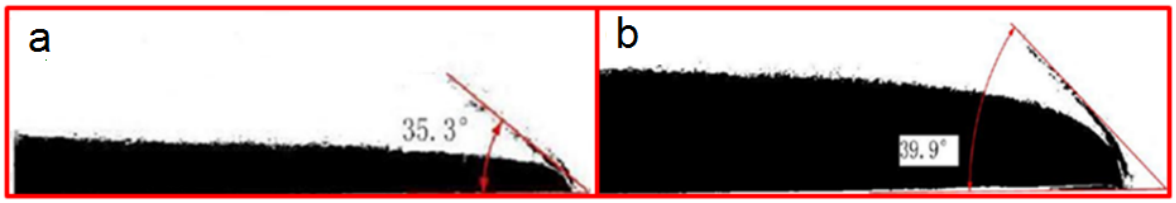

Fig.15. Measured angle of the shock wave of the kerosene jet under the different injection diameters (a) 0.4mm and (b) 1.0 mm [35]

Table 2 Pressure loss under different injection diameter

Injection diameter	Inlet pressure (Pa)	Outlet pressure (Pa)	Pressure loss (Pa)
D=0.5mm	785000	637495	147505
D=1.0mm	785000	617033	167967
D=1.5mm	785000	581672	203328

Based on the forgoing comparisons between published evidences and numerical results, though there are the discrepancies in magnitude, the findings in this study suggest that the predicted scale effects of the different injection diameters on mixing in the cold supersonic flow using the combined CLSVOF approach with improved K-H & R-T model are in qualitative agreement with the those in literature.

5. Conclusions

The scale effect of various injection sizes, in a cold kerosene-fueled scramjet combustor, on the interaction between incident shock wave and transversal cavity injection was studied using a combined three dimensional Couple

Level Set & Volume of Fluids (CLSVOF) approach with an improved K-H & R-T model. The numerical simulations were mainly focused on penetration depth, span expansion area, angle of shock wave and sauter mean diameter (SMD) distribution when the injection angle, velocity and pressure drop were all constant. This work demonstrates that the penetration height, span expansion area and shock wave angle of the kerosene droplets are separately increased with the injection size, and that the kerosene droplets are more prone to breakup and atomization at the outlet of the combustor for the orifice diameter of 1.5mm. The calculation predictions are compared against the reported experimental measurements and published literatures with good qualitative agreement. The results shown here demonstrate the great effect of kerosene-based injection size on the interaction between incident shock wave and transversal cavity injection in the scramjet combustor and the mixing characteristics in cold supersonic flow. However, the current results suggest further investigations. More work is required to quantitatively validate the obtained simulations based on Liu's experimental setup. The numerical results obtained in this study can provide the evidences for better understanding the underlying mechanism of kerosene atomization in cold supersonic flow and the scramjet design improvement.

Acknowledgments

The authors thank the reviewers for their hard work. And also the authors acknowledge financial support for this work from the National Natural Science Foundation of China (Grant No. 11272309, 51575003), Anhui Provincial Natural Science Foundation (Grant No.1508085ME71) and Key Project of Anhui Education Committee (Grant No. KJ2015A031).

References

[1] Takahiro Ukai, Hossein Zare-Behtsh, Kin Hing Lo, Konstantinos Kontis, Shigeru Obayashi, Effects of dual jets distance on mixing characteristics and flow path within a cavity in supersonic crossflow, International Journal of Heat and Fluid Flow.50(2014) 254–262.

[2] J.P. Drummond, M. Bouchez, C.R. McClinton, Overview of NATO background on scramjet technology, NASA techdoc. (2006) 20060020216.

T. Mai, Y. Sakimitsu, H. Nakamura, Y. Ogami, T. Kudo, H. Kobayashi, Effect of the incident shock wave interacting with transversal jet flow on the mixing and combustion, Proceedings of the Combustion Institute.(2011) 332335–2342.

[4] W. Huang, L. Ma, M. Pourkashanian, D.B. Ingham, S.B. Luo, Z.G. Wang, Parametric effects in a scramjet engine on the interaction between the air stream and the injection, Proceedings of the Institution of Mechanical Engineers, Part G:Journal of Aerospace Engineering. 226 (3) (2012) 294–309.

[5] T. Mai, Y. Sakimitsu, H. Nakamura, Y. Ogami, T. Kudo, H. Kobayashi, Effect of the incident shock wave interacting with transversal jet flow on the mixing and combustion, Proceedings Combustion Institute.33(2) (2011) 2335–2342.

[6] E. Erdem, K. Kontis, Numerical and experimental investigation of transverse injection flows, Shock Waves 20 (2)(2010) 103–118.

[7] A. Abdelhafez, A.K. Gupta, R. Balar, K.H. Yu, Evaluation of oblique and traverse fuel injection in a supersonic combustor, in: 43rd AIAA/ASME/SAE/ASEE Joint Propulsion Conference & Exhibit, OH, Cincinnati, AIAA Paper (2007) 2007–5026.

[8] W. Huang, Z.G. Wang, L. Yan, W.D. Liu, Numerical validation and parametric investigation on the cold flow field of a typical cavity-based scramjet combustor, Acta Astronautica. 80(2012) 132–140.

[9] S.H. Lee, Characteristics of dual transverse injection in scramjet combustor, Part 1: mixing, Journal of Propulsion and Power 22 (5) (2006) 1012–1019.

[10] A.S. Pudsey, R.R. Boyce, Numerical investigation of transverse jets through multi-port injector arrays in a

supersonic crossflow, AIAA Paper (2008) 2008-2517.

[11] L.S. Jacobsen, J.A. Schetz, W.F. Ng, Flowfield near a mulitiport injector array in a supersonic flow, Journal of Propulsion and Power 16 (2)(2000) 216–226.

[12] S.K. Cox-Stouffer, M.R. Gruber, Effects of injector yaws on mixing characteristics of aerodynamic ramp injectors, AIAA Paper (1999) 99–0086.

[13] A. Zang, T. Tempel, K. Yu, S.G. Buckley, Experimental characterization of cavity augmented supersonic mixing, AIAA paper (2005)2005–1423.

[14] C. Lada, K. Kontis, Experimental studies on transitional and closed cavity configurations including flow control, Journal of Aircraft. 47(2) (2010)723–730.

[15] C.D. Ghodke, J. Pranatharthikaran, G.J. Retaureau, S. Menon, Numerical and experimental studies of flame stability in a cavity stabilized hydrocarbon-fueled scramjet, AIAA paper (2011)2011–2365.

[16] Wei-Lai Liu, Laser dropsizing of kerosene injected into a supersonic airstream, the project supported by the National Natural Science Foundation of China (Grant No.11272309)

[17] Lin Zhu, Xi-Cheng, Shuang-Shuang Peng, Yin-Yin Qi, Wen-Feng Zhang, Rui Jiang, Chen-Long Yin,Three dimensional computational fluid dynamic interaction between soil and plow-breast of horizontally reversal plow, Computers and Electronics in Agriculture .123(2016)1–9.

[18] Lawson,S.J.,Barakos,G.N., Review of numerical simulations for high-speed, turbulent cavity flows. Prog. Aerosp. Sci. 47(2011)186–216.

[19] Ukai, T., Zare-Behtash, H., Erdem, E., Lo, K.H., Kontis, K., Effectiveness of jet location on mixing characteristics inside a cavity in supersonic flow, Exp.Therm. Fluid Sci. 54(2014)59–67.

[20] Olsson E, Kreiss G. A conservative level set for two phase flow, Journal of computational physics. 210(2005) 225–246.

[21] Zhao Yu, Yang Ge, and L.-S. Fan, Multi-scale simulation of oblique collision of a droplet on a surface in the Leiden-frost regime, Chemical Engineering Science 62 (2007) 3462-3472.

[22] T. Mènard S. Tanguy, A. Berlemont, Coupling level set/VOF/ghost fluid methods: validation and application to 3D simulation of the primary break-up of a liquid jet, International Journal of Multiphase Flow 33 (2007) 510-524.

[23] Nickolay N.Smirnov, Valeriy F. Nikitin, Vladislav R. Dushin, Yurii G. Filippov, Valentina A. Nerchenko, Javad Khadem. Combustion onset in non-uniform dispersed mixtures, Acta Astronautica, 155(2015) 94-101.

[24] V.B.Betelin, V.F.Nikitin, A.G.Kushnirenko, V.A. Nerchenko, N.N.Smirnov. Spray injection and ignition in a heated chamber modeling, WSEAS Trans Fluid Mech. 1790-50876 3(2011)147-159.

[25] V.B.Betelin, N.N.Smirnov, V.F.Nikitin,V.R.Dushin, A.G.Kushnirenko, V.A. Nerchenko. Evaporation and ignition of droplets in combustion chambers modeling and simulation, 70 (2012) 23-35.

[26] F.R.Menter, M.Kuntz, R.Langtry. Ten years of experience with the SST turbulence model, Heat and Mass Transfer, 4, Begell House Inc 2003, 625~632.

[27] W.Huang. Design exploration of three-dimensional transverse jet in a supersonic crossflow based on data mining and multi-objective design optimization approaches. International Journal of Hydrogen Energy 39 (2014), 3914~3925.

[28] W. Huang, W.D. Liu, S.B. Li, Z.X. Xia, J. Liu, Z.G. Wang, Influences of the turbulence model and the slot width on the transverse slot injection flow field in supersonic flows, Acta Astronautica 73(2012) 1–9.

[29] Driscoll R, St George A, Gutmark E, Numerical investigation of injection within an axisymmetric rotating detonation engine, International Journal of Hydrogen Energy, 41(2016) 2052–2063.

[30] A. I. Glagolev, A, I. Zubkov, and Yu. A. Panov, supersonic flow past a gas let obstacle emerging from a plate, Fluid dynamic. 2(3) (1967)97–102.

[31] Joseph D.D., Belanger J., Beavers G.S., Breakup of a liquid drop suddenly exposed to a high-speed airstream.

International Journal of Multiphase Flow, 25 (1999) 1263-1303.
[32] Jing Liu. Numerical and experimental investigation of fuel spray in supersonic cross flow. PhD dissertation, Beihang University, Beijing, China, 2010.
[33] Nickolay N.Smirnov, Valeriy F. Nikitin, Vladislav R. Dushin, Yurii G. Filippov, Valentina A. Nerchenko, Javad Khadem. Combustion onset in non-uniform dispersed mixtures, Acta Astronautica, 155(2015) 94-101.
[34] Reitz R.D., Diwaker R.. Structure of high pressure fuel sprays, (1987) SAE870598.
[35] Yi-Heng Tong, Injection characteristic and breakup process of transversal liquid jet in crossflow, Master thesis, National University of Defense Technology, P.R.China (2012).
[36] A. I. Glagolev, A, I. Zubkov, and Yu. A. Panov, Interaction between a supersonic flow and gas issuing from a hole in a plate, Fluid dynamic. 8(2) (1968)99-103.